Photonic Microresonator Based Sensor for Selective Nitrate Ion detection

Zhongbo Zhang[a,*], Xufeng Zhang[b], Tijana Rajh[b], and Supratik Guha[a]

[a] *Pritzker School of Molecular Engineering, the University of Chicago, Chicago, IL 60637, United States*

[b] *Center for Nanoscale Materials, Argonne National Laboratory, Argonne, IL 60439, United States*

Corresponding author email: zxz202@uchicago.edu (Z. Zhang)

Abstract

Sensing nitrate concentrations in soil with high sensitivity and selectivity using field deployable compact sensor platforms are a sought-after goal for environment and agriculture applications. This study demonstrates a new optically based nitrate sensing platform based on ion-selective membrane (ISM) functionalized chip-scale photonic micro-ring resonators. Our approach relies upon measurements of resonance shifts in the micro-resonators and leverages the excellent, though little studied, optical properties of ISMs. Using a high-quality micro-ring resonator, a nitrate ion-selective photonic sensor exhibits a detection limit down to 0.1 parts per million (ppm) and enables nitrate concentration measurements in the 1-100 ppm level, appropriate for soil science and agriculture. Importantly, the sensor also shows high selectivity over other competing anions in soil, such as Cl^- and NO_2^-. We argue that this chip-scale approach can be incorporated into compact sensor platforms.

Keywords: Nitrate sensor, Micro-ring resonator, ion selective membrane, integrated photonic sensor

1. Introduction

Highly selective chemical sensing of the nitrate ion at trace levels is an important research topic for a broad range of areas from environmental sensing and soil science, to agriculture and homeland security. Nitrate is a key mineral nutrient for most plants, and its application via fertilizers is a major source of water pollution globally due to fertilizer runoff in rivers and streams [1,2]. Precision nitrogen-management and efficient fertilization can reduce the negative impact to the environment, and is desirable in modern agriculture [3]. High resolution measurements of soil nitrate concentration (10-100 ppm is the relevant range) is also key to a better understanding of the biogeochemistry of soils and its impact on plant growth. However, a reliable field-deployed sensor technology for effectively detecting the concentration of such ions at high sensitivity, specificity and accuracy is still lacking. In-situ, compact sensing approaches relevant to nitrate detection can be categorized into two types: potentiometric methods and optical methods. For potentiometric approaches such as the ion-selective electrode (ISE) [4-6] and the ion-selective field-effect transistor (ISFET) [7,8], the intrinsic potential drift from a reference electrode cannot be avoided and the need for frequent calibration can hinder their practical applications, especially for soil sensing [9]. In contrast, optical sensing approaches for detecting nitrates may need no reference element, and minimal electrical interference and baseline variation can be eliminated [10]. Spectrophotometric methods are well studied for nitrate/nitrite determination, including UV-vis [11,12], fluorimetric [13,14], and chemiluminescence [15]. However, these techniques need complicated sample pretreatment, such assay protocols involving redox reactions, which are unfavorable for field-deployed nitrate determination [10]. Other optical methods such as Fourier-transform infrared spectroscopy (FT-IR) [16,17] and Raman spectroscopy [18] for detecting nitrate have also been evaluated. Although these methods can provide outstanding sensitivity, the need

for sophisticated and expensive instrument reduces the interest in these techniques beyond the laboratory.

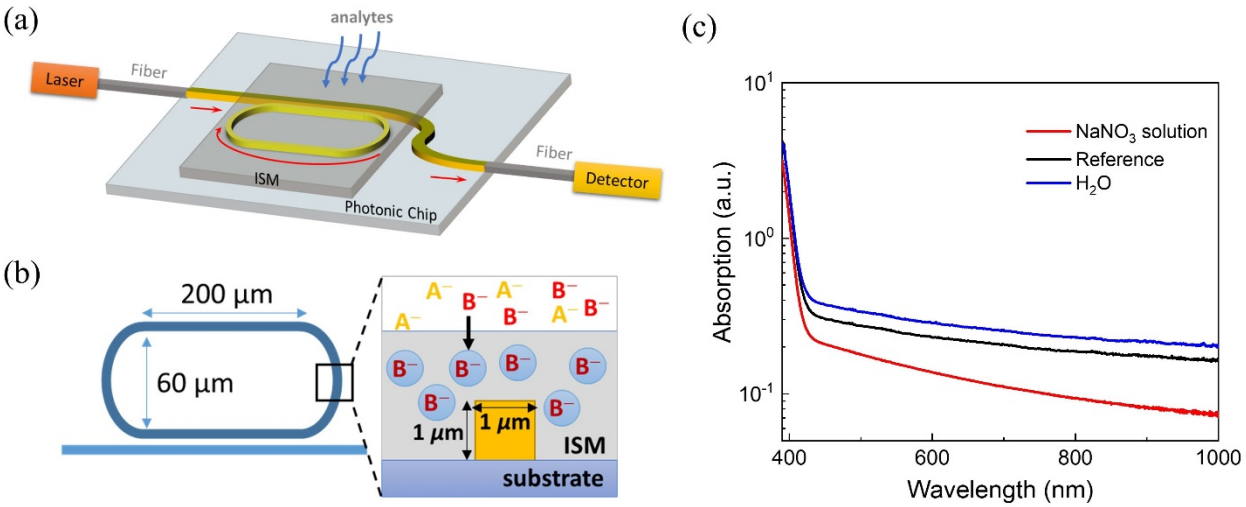

Fig. 1. (a) Schematics of the nitrate ion-selective photonic sensor. (b) Cross-sectional view of the device. ISM coating covers the micro-ring resonator and isolate the photonic device from the solution environment. The presence of the ionophore ensures only the target ions can be bond and diffuse within the membranes and affect the optical response. (c) UV-Vis transmission spectrum of a 100-µm-thick nitrate ISM with different soaking conditions: no soaking (black line), soaked in water overnight (blue line), and soaked in sodium nitrate solution overnight with a concentration of 1000 ppm (red line).

Compared with other optical methods, silicon-based integrated photonic sensors are well known for their advantages of compact size and multiplexed sensing capability [19, 20]. Our research targets the development of small, low-cost, high-sensitivity micro-ring resonator-based photonic sensor platforms fabricated on silicon (Fig. 1a) capable of sensing ionic species such as nitrates. Such evanescently coupled resonator structures enable the detection (using refractometry measurements) of small shifts (~10^{-3}-10^{-4}) in refractive indices that embeds the resonator surface.

Our strategy is to functionalize this embedding media with materials that can selectively bind to the target analyte, assuring high specificity in the sensing process. The selective binding results in a change in the refractive index which is picked up by shifts in the light absorption peak through the resonator device. In this paper, we demonstrate the feasibility of this technique for nitrate sensing. Using nanofabricated micro-ring resonators integrated with nitrate selective polymer films that undergo small but detectable changes in the refractive index upon absorbing nitrate ions, we show that nitrate concentrations in the relevant range of 10-100 ppm can be detected with good specificity against Cl^- and NO_2^-. These targets appropriately meet the needs for nitrate sensors geared towards soil and plant science. To our knowledge, integrated photonic sensors for nitrates have not been reported in the literature before.

The polymer films used for functionalization are ion-selective membranes (ISMs). While nitrate ISMs were exploited in techniques that monitor electrical signals [21,22], such as potentiometric thick film sensors [23,24] and ion-selective field-effect transistors (ISFETs) [7,8], ISMs are also excellent optical materials and their optical properties have not been well explored thus far. ISMs can be prepared in a polyvinyl chloride (PVC)-based polymer matrix, which is typically transparent in the visible light regime and can be integrated as optical coatings. Research on the optical properties of ISMs has been limited [25], and, while there have been some applications using ISMs in optical sensors [26], ISMs have not been adopted in highly sensitive photonic microresonators that rely on their optical refractive index response [27].

2. Results and Discussion

2.1 Optical Properties of ISM.

The nitrate ion-selective membrane used in this work is composed of tridodecylmethylammonium nitrate (TDDMA) dispersed in over-plasticized PVC polymer matrix. The ionophore TDDMA serves as a selective ion carrier which allows only nitrate ions enter the hydrophobic membrane from the aqueous solution (Fig. 1b). This nitrate ionophore were widely used for preparing nitrate ion-selective membrane and has been proven to have excellent selectivity for nitrate ions when adopted in ISE and ISFET applications [28-29]. The membrane is prepared from the premixed cocktail solutions containing TDDMA, plasticizer, additives, and PVC that are all dissolved in tetrahydrofuran (THF) solvent.

To demonstrate the feasibility of using TDDMA ISM as the functionalization layer for a photonic sensor, the optical properties of 100-μm-thick membranes were first studied. The samples were soaked overnight in either a de-ionized (DI) water solution (as a control sample), or a solution of sodium nitrate (with a concentration of 1000 ppm), respectively. From the UV-Vis measurements of optical absorption (Fig. 1c), it is clearly observed that the ISMs show low absorption in the visible light regime. The absorption coefficient of the ISM changes abruptly around ~420 nm in all three cases. We believe this is due to the optical absorption characteristics of the PVC polymer matrix. For the control sample soaked in DI water, the absorption increases slightly after the soaking. For the sample soaked in the nitrate solution, the membrane absorption is reduced by a factor of three after the soaking. When the ISM is used as a functionalization coating on highly sensitive photonic devices, such a slight absorption change can be captured with high precision. According to the Kramers-Kronig relation, such a change in absorption over a broad spectral range will also result in a change in the ISM's refractive index. The refractive index change can be read out using refractometric measurement, which is more reliable than the absorption-based sensing techniques as it relies on spectral information that is less susceptible to

external interferences. Therefore, this ISM is intrinsically a good candidate as a functionalization coating for integrated photonic sensors that can measure small changes in the refractive index. Combined with the high sensitivity of photonic sensing platforms, and using nitrate detection as an example, we show in this work that trace-level detection of ions can be achieved.

2.2 Device Fabrication, Simulation, and Characterization.

The device fabrication flow is described in Fig. 2a. Numerical simulations (Finite-Difference Time-Domain method using the Lumerical software package) of our micro-resonator device shows that the square-shaped waveguide cross-section supports one fundamental transverse electric (TE) and one transverse magnetic (TM) mode [30]. A race-track-type ring resonator is used where the micro-ring resonator and the waveguide are aligned in parallel along a length of 200 μm to ensure good coupling between the micro-ring resonator and the waveguide. A bending radius of 30 μm was used in order to achieve a balance between low optical loss (small bend radius results in high optical loss), and a large free spectral range (FSR, i.e., spectral separation of two neighboring resonances) which reduces as the bend radius increases. Ideally, the FSR should be significantly larger than the resonance shift due to the analyte detection. An optimal gap between the micro-ring and the waveguide of around 350 nm was chosen by comparing and selecting the highest extinction ratios from a set of devices with gaps varying from ~100 – 600 nm.

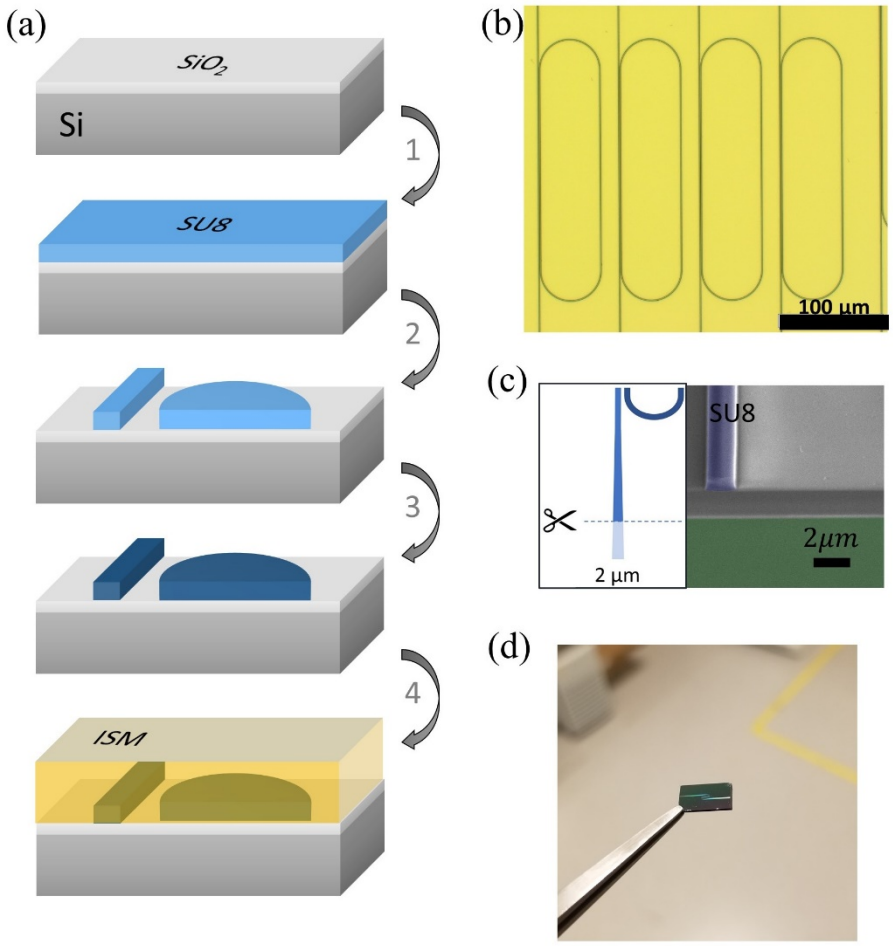

Fig. 2. (a), Device fabrication procedure. Step 1: spin coating of SU8; Step 2: electro-beam lithography and developing; Step 3: hard baking for SU8 curing; Step 4: application of the ISM to the chip surface; (b), Optical image of the fabricated SU8 micro-ring resonator; (c), Scanning electron microscopy (SEM) image of the SU8 waveguide cross-section and schematic for the tapered waveguide; (d), Image of a photonic sensor chip.

Transmission measurements are carried out by sending light from a tunable external-cavity laser through the device and monitoring the output light spectrum while the input light wavelength is scanned. A typical measured transmission spectrum of a micro-resonator is shown in Fig. 3a. A series of optical resonance dips are observed in the transmission spectrum at wavelengths that

satisfy the resonance condition $\lambda = n_{\text{eff}} \times L/m$, where λ is the resonance wavelength, n_{eff} is the effective index of the waveguide mode, L is the total length of the micro-ring and m is an integer mode index. The micro-resonator has a total length of 526 μm, corresponding to a FSR of 0.60 nm. The coupling gap between the micro-resonator to the waveguide is optimized to obtain a large extinction ratio. Because of the square shape of the waveguide cross-section, the two modes, TE and TM, are almost degenerate and their FSRs are very similar. According to $\lambda = n_{\text{eff}} \times L/m$, the sensitivity can be calculated as $d\lambda/dn \approx d\lambda/dn_{eff} = \lambda/n_{eff}$, assuming n_{eff} is the refractive index of SU8 (1.564). The estimated sensitivity of such microresonators is 500 nm/RIU (RIU: refractive index unit). Without the ISM coating, the microresonator transmission spectrum shows a series of narrow resonance dips (Fig. 3a) with a linewidth ~8pm which corresponds to a loaded Q-factor of 96,000 as shown in Fig. 3b, which is a zoomed in section from Fig. 3a. The deep, nearly symmetric curve can be well fitted by a Lorentzian function, indicating a high sensitivity and a large ratio of resonance signal/background noise. Due to the high spectral resolution of the tunable laser, sub-pm shifts in the optical resonance can be resolved, which corresponds to an approximate change of 1e-4 in refractive index according to the equation $\lambda = n_{\text{eff}} \times L/m$.

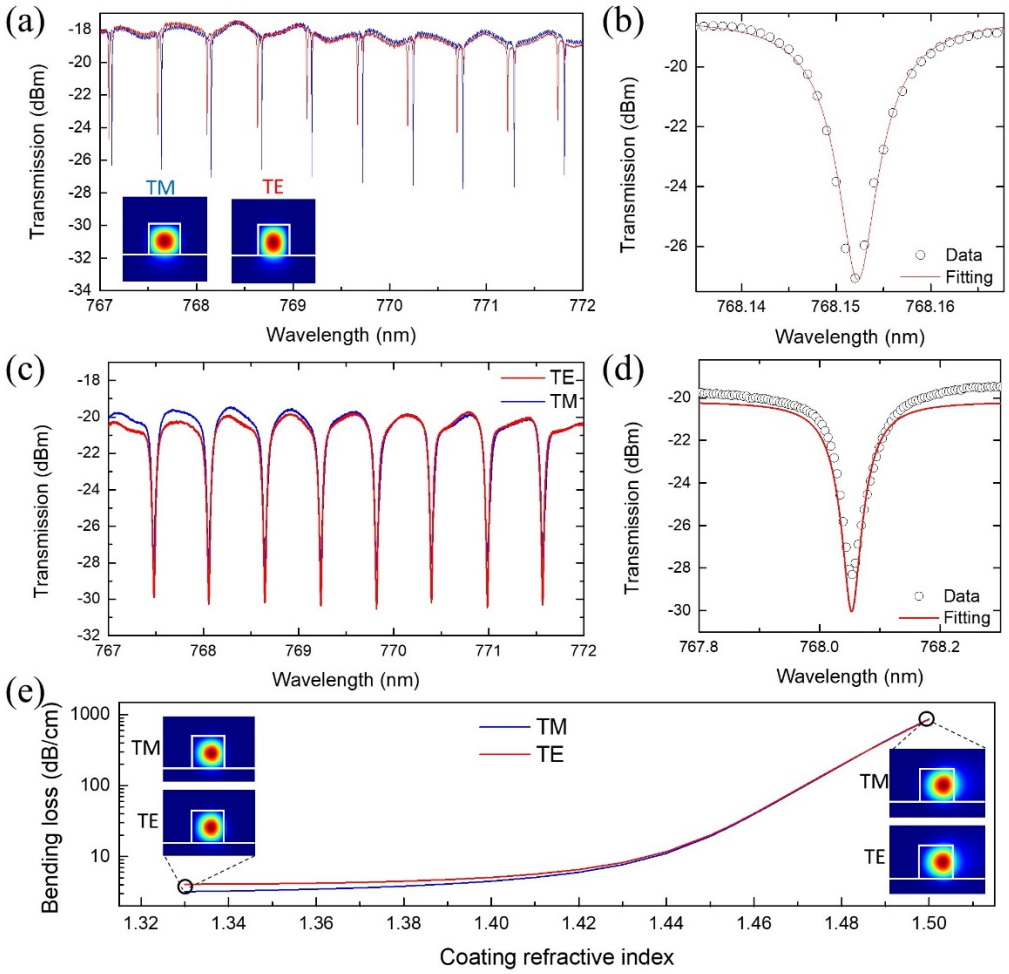

Fig. 3. (a) Experimental optical transmission spectrum of a microresonator without a functionalization coating; Inset of (a) shows the magnetic field distribution of the transverse-electric (TE) and transverse-magnetic (TM) modes; (b) Zoomed-in spectrum of one optical resonance, showing a linewidth of 8 pm; (c) Experimental optical transmission spectrum of a microresonator with a 100 nm ISM coating; (d) Zoomed-in spectrum of one optical resonance for the functionalized device; The spectra in (b) and (d) are fitted to a Lorentzian lineshape; (e) Bending loss of a $1\times1\mu m^2$ SU8 waveguide (with a bending radius of 30 μm) as a function of refractive index of the functionalization coating at 770 nm wavelength; Inset of (e) shows the magnetic field distribution of the TE and TM modes at n = 1:33 (low bending loss) and n = 1:50 (high bending loss), respectively.

The application of the ISM to the photonic chip surface alters the local refractive index near the micro-ring resonator and therefore affects the transmission spectrum. Fig. 3c shows the resonance spectrum of the micro-ring resonator with the ISM coating. The ISM membrane has a refractive index around 1.52, resulting in slightly increased FSRs (0.61 nm). On the other hand, the increase of the refractive index in the cladding (i.e. the ISM membrane) also causes increased bending losses for small micro-rings. Optical simulations of Finite-Difference Time-Domain method using Lumerical indeed show that the optical bending loss increases from 3 dB/cm to 800 dB/cm when the coating refractive index increases from 1.33 to 1.50 for a bending radius of 30 μm. From the magnetic field distribution (insets of Fig. 3e) of the ring cross-section, it is evident that the mode leaks out when the refractive index of the coating is very close to that of the SU8 waveguide (1.564 at 765 nm). Besides, the ISM coating introduces additional absorption losses that lead to a decreased Q factor of 10,000. The functionalized micro-ring resonators still exhibits a nearly symmetric resonance peak with a somewhat broader resonance with a linewidth of around 80 pm, as shown in Fig. 3c and d. This determines a measurable refractive index change of ~1e-3.

2.3 Nitrate Ion-Concentration Sensing.

The response of a functionalized micro-ring resonator device to the presence of nitrate ions was studied by refractometry measurements. During the measurement, the laser wavelength is set to continuously sweep over a 3 nm range, started at 765 nm at constant power and the transmission spectra are recorded in real time. Initially, nitrate ionophore-cocktail A, i.e. the commercial ISM cocktail used for potentiometric sensing approaches, was used as-received to functionalize the micro-ring photonic sensor with a coating thickness of ~100 nm. Multiple resonances are observed

within the measured wavelength range (Fig. 3c), and the redundancy provides additional reliability by averaging the results from different resonances. When the photonic sensor is exposed to nitrate solutions with different concentrations, the refractive index of the ISM coating changes due to the ion diffusion into the membrane from the aqueous phase, which in turn results in a shift in the optical resonance wavelength of the micro-resonator. However, the sensor functionalized by the commercial ISM cocktail exhibited poor sensitivity, i.e., the total resonance shift is only 0.3 Å when varying the nitrate concentration from 0.02 ppm to 109 ppm, as shown in Fig. S1.

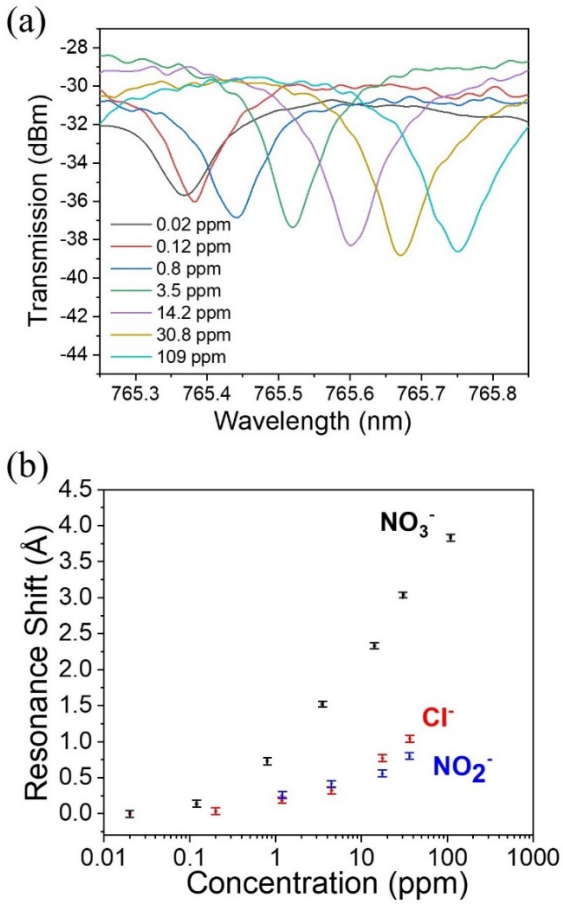

Fig. 4. (a) Optical transmission spectrum of a nitrate-ISM-functionalized in nitrate solutions with difference concentration; (b) Resonance shift as a function of ion concentration in three different solutions. Error bars are obtained based on five parallel wavelength scans.

To enhance the sensitivity, the concentration of the nitrate ionophore in the ISM membrane was increased from 1.5 wt.% to 6.2 wt.% by adding additional TDDMA to the precursor cocktail solution. A higher ionophore concentration can lead to larger changes in the refractive index of the functional coating upon changing the nitrate concentration. Further increasing the ionophore content however can lead to the ionophore precipitation during the drying process. By pipetting sodium nitrate solutions onto the photonic sensor, the nitrate concentration is continuously varied from 0.02 ppm to 109 ppm. Fig. 4 shows the refractometric measurement results as a function of solution concentration. With respect to the standard solution containing 0.02 ppm sodium nitrate, a resonance shift was clearly observed at a concentration as low as 0.1 ppm. Each test was performed under the controlled experimental condition where the optical transmission spectrum was continuously recorded within a given exposure time of 5 mins after each concentration adjustment. For each test, the resonance dip gradually shifted and always stabilized within 4 minutes (Fig. S2), indicating the relatively fast response of this ISM-functionalized photonic sensor. With the nitrate concentration increasing, the optical resonances shift towards longer wavelengths, implying an increased refractive index. The optical resonances are directly correlated with the nitrate concentration. Numerical fitting gives a relationship of $S = 1.472*\log N + 0.783$, where S is the resonance shift in a unit of Å, while N is the nitrate concentration in a unit of ppm. In this case the shift is 3 Å for a nitrate concentration change from 1 ppm to 100 ppm, significantly higher than the case of the commercial ISM precursor cocktail. This integrated photonic sensor shows an unambiguous correlation with the nitrate concentration within the relevant range of nitrate detection desirable for soil science (~few to ~100 ppm), ensuring a satisfactory detection range comparable to ISEs. Note that the highly sensitive microresonator-based photonic device captures resonance dips with high resolution while providing repeatable, consistent results. As

shown in Fig. S3, when the nitrate concentration is fixed, the resonance dip barely changes in position during wavelength sweeping for 10 cycles over a 4 Å range. The standard deviation of the resonance shift was calculated to be ± 0.6 pm, and corresponds to a resolution of approximately ~1 ppm in terms of uncertainty in the nitrate concentration. Coupled with the high-spectral-resolution tunable laser that can resolve the sub-pm shift in the optical resonance, the nitrate concentration can be accurately determined using the integrated photonic sensor. Compared with ISEs that can suffer from degraded accuracy caused by the intrinsic potential drift from a reference electrode,[31] the integrated photonic sensor shows potential advantages in terms of accuracy and stability of measurement. Note that the resolution of ~1 ppm is obtained under laboratory settings with laboratory grade equipment. Under field conditions, for in-situ sensing, we anticipate that compact optical setups based upon portable tunable lasers will be used. The resolution may be lower under such circumstances. This is the subject of further study and is outside the scope of this investigation.

The use of thicker ISM films results in a continual drift of the resonance peak position without stabilizing within 10 minutes of the start of the test. The results are shown in Fig. S4 in the supplemental section. This can be attributed to the slow diffusion process from the aqueous solution to the hydrophobic plasticized polymer phase. For practical use, a quick and stable response is preferred. Therefore, a thin film layer of ISM (e.g., 100 nm) is more suitable as the functionalization coating for microresonator photonic sensors.

To investigate the selectivity of such ion-selective microresonator sensors, control experiments were then carried out using sodium solutions with Cl^- and NO_2^-. The Cl- ion widely exists in agricultural soil and water in a concentration of tens to hundreds ppm, comparable with the nitrate concentration in the environment. Because of the strong similarity between chloride and

nitrate anions in terms of their hydrated radius and charge, differentiating between Cl^- and NO_3^- by common sensor techniques is always challenging. On the other hand, a nitrate sensor is required to show selectivity over nitrite ions, since for agricultural studies purposes the nitrate concentration is of importance (roots absorb nitrates and not nitrites). The measurement results of selectivity are shown in Fig. 4b. Unlike the case for the nitrate solutions, the correlation between the resonance shift and the anion concentrations of NO_2^- and Cl^- is negligible when the concentration is below 10 ppm. When exposing to a solution with a concentration above 10 ppm, the photonic sensor maintains an excellent selectivity for nitrate, where the resonance shift is four times larger than that of the other anions at the same concentration.

3. Conclusions

To summarize, we have demonstrated a chip-scale photonic sensing platform for nitrate ion sensing with high sensitivity and specificity when it is coated with a nitrate-selective ISM as a functionalizing membrane. Our study shows that the ISM serves as a low absorption loss optical coating whose refractive index changes as a function of nitrate content. These small changes are detected via shifts in the resonance peaks of the ring-microresonator structure based photonic device. The device is exposed to sodium nitrate solutions of various concentrations, and the measured resonance shift shows an unambiguous correlation with the nitrate concentration from between 1-100 ppm, a nitrate detection sensitivity of 0.1 ppm, and good specificity against Cl^- and NO_2^- ions. The shifts themselves, are within the reach of compact solid-state lasers (such as distributed feedback lasers) and detectors so that this approach may be suitable for compact field deployable units using integrated photonic technologies. Using the functionalized membranes, our experiments also demonstrate a new approach for utilizing ISMs for sensing applications,

providing new opportunities in sensing for not only nitrate ions but a wide range of ions where ISMs are available.

Acknowledgement

This work was performed at the Center for Nanoscale Materials, a U.S. Department of Energy Office of Science User Facility, and supported by the U.S. Department of Energy, Office of Science, under Contract No. DE-AC02-06CH11357. The authors thank Dr. Ralu Divan and Dr. Leonidas Ocola for helping in device fabrication, and Dr. Houcheng Chang for helping with the functionalization coating. This research was funded in part by National Science Foundation (Award No. 1841652).

Supporting Information.

Experimental Section; refractometric measurement results for the photonic sensor functionalized by commercial nitrate ionophore cocktail; study for response time of the photonic sensor; study for precision of the photonic sensor; refractometric measurements of the photonic sensor functionalized by thick ISM.

References

[1] H. Di, K. Cameron, How does the application of different nitrification inhibitors affect nitrous oxide emissions and nitrate leaching from cow urine in grazed pastures? Soil Use Manage 28 (2012) 54-61. https://doi.org/10.1111/j.1475-2743.2011.00373.x

[2] J. Dymond, A. G. Ausseil, R. Parfitt, A. Herzig, R. McDowell, Nitrate and phosphorus leaching in new zealand: a national perspective. New Zealand J. Agricultural Res. 56 (2013) 49-59. https://doi.org/10.1080/00288233.2012.747185

[3] V. I. Adamchuk, J. W. Hummel, M. T. Morgan, S. K. Upadhyaya, On-the-go soil sensors for precision agriculture. Computers and Electronics in Agriculture 44 (2004) 71–91. https://doi.org/10.1016/j.compag.2004.03.002

[4] D. Wegmann, H. Weiss, D. Ammann, W. E. Morf, E. Pretsch, K. Sugahara, W. Simon, Anion-selective liquid membrane electrodes based on lipophilic quaternary ammonium compounds. Microchimica Acta 84 (1984) 1–16. https://doi.org/10.1007/BF01204153

[5] A. S. Watts, V. G. Gavalas, A. Cammers, P. S. Andrada, M. Alajarin, L. G. Bachas, Nitrate-selective electrode based on a cyclic bis-thiourea ionophore. Sensors and Actuators B 121 (2007) 200–207. https://doi.org/10.1016/j.snb.2006.09.048

[6] A. Seichi, N. Kozuka, Y. Kashima, M. Tabata, T. Goda, A. Matsumoto, N. Iwasawa, D. Citterio, Y. Miyahara, K. Suzuki, Real-time monitoring and detection of primer generation-rolling circle amplification of DNA using an ethidium ion-selective electrode. Anal Sci. 32 (2016) 505-510. https://doi.org/10.2116/analsci.32.505

[7] L. Campanella, C. Colapicchioni, G. Crescentini, M. Sammartino, Y. Su, M. Tomassetti. Sensitive membrane isfets for nitrate analysis in waters. Sensors and Actuators B: Chemical 27 (1995) 329–335. https://doi.org/10.1016/0925-4005(94)01612-L

[8] C. Jimenez-Jorquera, J. Orozco, A. Baldi, ISFET based microsensors for environmental monitoring. Sensors 10 (2010) 61–83. https://doi.org/10.3390/s100100061

[9] D. Yu, Y. Wei, G. Wang, Time-dependent response characteristics of ph-sensitive ISFET. Sensors and Actuators B 3 (1991) 279–285. https://doi.org/10.1016/0925-4005(91)80018-F

[10] M. J. Moorcroft, J. Davis, R. G. Compton, Detection and determination of nitrate and nitrite: a review. Talanta 54 (2001) 785-803. https://doi.org/10.1016/S0039-9140(01)00323-X

[11] H. W. Jannasch, K. S. Johnson, C. M. Sakamoto, Submersible, osmotically pumped analyzer for continuous determination of nitrate in situ. Analytical Chemistry 66 (1994) 3352-3361. https://doi.org/10.1021/ac00092a011

[12] M. Huebsch F. Grimmeisen, M. Zemann, O Fenton, K. Richards, P. Jordan, A. Sawarieh, P. Blum, N. Goldscheider, Technical notes: field experience using uv/vis sensors for high-resolution monitoring of nitrate in ground water. Hydrology and Eearth System Sciences 19 (2015) 1589–1598. https://doi.org/10.5445/IR/1000046934

[13] M. Hidaka, A. Gotoh, T. Shimizu, K. Minamisawa, H. Imamura, T. Uchida, Visualization of NO_3^-/NO_2^- dynamics in living cells by fluorescence resonance energy transfer (FRET) imaging employing a rhizo-5 bial two-component regulatory system. Journal of Biological Chemistry 29 (2016) 2260–2269. https://dx.doi.org/10.1074%2Fjbc.M115.687632

[14] A. Buldt, U. Karst, U. Determination of nitrite in waters by microplate fluorescence spectroscopy and HPLC with fluorescence detection. Analytical Chemistry 71 (1999) 3003–3007. https://doi.org/10.1021/ac981330t

[15] M. Yaqoob, B. Biot, A. Nabi, P. Worsfold, Detection of nitrate and nitrite in freshwaters using flow-injection with luminol chemiluminescence detection. Luminescence 27 (2012) 419–425. https://doi.org/10.1002/bio.1366

[16] A. Shaviv, A. Kenny, I. Shmulevitch, L. Singher, Y. Raichlin, A. Katzir, Direct Monitoring of soil and water nitrate by FTIR based FEWS or membrane systems. Environmental Science and Technology 37 (2003) 2807–2812. https://doi.org/10.1021/es020885+

[17] M. Trivedi, A. Branton, D. Trivedi, G. Nayak, K. Bairwa, S. Jana, Spectroscopic characterization of disodium hydrogen orthophosphate and sodium nitrate after biofield treatment. Chromatography Separation Techniques 6 (2015) 1000282. http://dx.doi.org/10.4172/2157-7064.1000282

[18] A. Ianoul, T. Coleman, S. Asher, UV resonance raman spectroscopic detection of nitrate and nitrite in wastewater treatment processes. Analytical Chemistry 74 (2002) 1458–1461. https://doi.org/10.1021/ac010863q

[19] N. A. Yebo, P. Lommens, Z. Hens, R. Baets, An integrated optic ethanol vapor sensor based on a silicon-insulator microring resonator coated with a porous ZnO film. Opt. Express 18 (2010) 11859-11866. https://doi.org/10.1364/OE.18.011859

[20] K. Xu, Y. Chen, T. A. Okhai, L. W. Snyman, Micro optical sensors based on avalanching silicon light-emitting devices monolithically integrated on chips. Optical Materials Express 10 (2019) 3985-3997. https://doi.org/10.1364/OME.9.003985

[21] S. Wakida, M. Yamane, A. Kawahara, S. Takasuka, K. Higashi, Durable poly(vinyl chloride) matrix ion-selective field effect transistors for nitrate ions. Bunseki Kagaku 38 (1989) 510-514. https://doi.org/10.2116/bunsekikagaku.38.10_510

[22] M. Knoll, K. Cammann, C. Dumschat, C. Sundermeier, J. Eshold, Potentiometric silicon microsensor for nitrate and ammonium. Sensors and Actuators B 18 (1994) 51–55. https://doi.org/10.1016/0925-4005(94)87055-1

[23] M.Gartia, B. Brauschweig, T. W. Chang, P. Moinzadeh, B. Minsker, G. Agha, A. Wieckowski, L. Keefer, G. Liu, The microelectronic wireless nitrate sensor network for environmental water monitoring. Journal of Environmental Monitoring 14 (2012) 3068. https://doi.org/10.1039/c2em30380a

[24] J. Artigas, C. Jimenez, S. G. Lemos, A. Nogueira, A. Torre-Neto, J. Alonso, Development of a screen-printed thick-film nitrate sensor based on a graphite-epoxy composite for agricultural applications. Sensors and Actuators B 88 (2003) 337–344. https://doi.org/10.1016/S0925-4005(02)00399-4

[25] D. Freiner, R. Kunz, D. Citterio, U. Spichiger, M. Gale, Integrated optical sensors based on refractometry of ion-selective membranes. Sensors and Actuators B 29 (1995) 277–285. https://doi.org/10.1016/0925-4005(95)01694-5

[26] X. Xie, M. Pawlak, M. Tercier-Waeber, E. Bakker, Direct optical carbon dioxide sensing based on a polymeric film doped with a selective molecular tweezer-type ionophore. Analytical Chemistry 84 (2012) 3163-3169. https://doi.org/10.1021/ac2030046

[27] G. Kim, K. Sudduth, S. Grant, N. Kitchen, Disposable nitrate-selective optical sensors based on fluorescent dye. Journal of Biosystems Engineering 37 (2012) 209–213. https://doi.org/10.5307/JBE.2012.37.3.209

[28] M. Knoll, K. Cammann, C. Dumschat, C. Sundermeier, J. Eshold, Potentiometric silicon microsensor for nitrate and ammonium. . Sensors and Actuators B: Chemical 18 (1994) 51–55. https://doi.org/10.1016/0925-4005(94)87055-1

[29] M. Knoll, K. Cammann, C. Dumschat, J. Eshold, C. Sundermeier, Micromachined ion-selective electrodes with polymer matrix membranes. Sensors and Actuators B: Chemical 21 (1994) 71–76. https://doi.org/10.1016/0925-4005(94)01227-X

[30] K. Xu, Monolithically integrated Si gate-controlled light-emitting device: science and properties. Journal of Optics 20 (2018) 024014. https:// doi: 10.1088/2040-8986/aaa2b7

[31] B. A. Pellerin, B. A. Bergamaschi, B. D. Downing, J. F. Saraceno, J. D. Garrett, L. D. Olsen, Optical techniques for the determination of nitrate in environmental waters: Guidelines for instrument selection, operation, deployment, maintenance, quality assurance, and data reporting, in: Collection of Water Data by Direct Measurement, Geological Survey, 2013, pp. 1-37. https://doi.org/10.3133/tm1D5

Supporting Information

Photonic Microresonator Based Sensor for Selective Nitrate Ion detection

Zhongbo Zhang[a,*], Xufeng Zhang[b], Tijana Rajh[b], and Supratik Guha[a]

[a] *Pritzker School of Molecular Engineering, the University of Chicago, Chicago, IL 60637, United States*

[b] *Center for Nanoscale Materials, Argonne National Laboratory, Argonne, IL 60439, United States*

Table of Content

1. Experimental Section

2. Refractometric Measurement Results for the Photonic Sensor Functionalized by Commercial Nitrate Ionophore Cocktail

3. Study for Response Time of the Photonic Sensor

4. Study for Precision of the Photonic Sensor

5. Refractometric Measurements of the Photonic Sensor Functionalized by Thick ISM

1. Experimental Section

Chemicals. Sodium nitrate, tridodecylmethylammonium nitrate (TDDMA), tetrahydrofuran, and nitrate ionophore-cocktail A are purchased from Sigma-Aldrich and used as received. The composition of the commercial nitrate ionophore cocktail A is: methyltriphenylphosphonium bromide (0.25 wt. %), nitrocellulose (1.93 wt.%), 2-nitrophenyl octyl ether (16.25 wt.%), poly(vinyl chloride) (5.75 wt.%), tetrahydrofuran (74.32 wt.%), tridodecylmethylammonium nitrate (1.5 wt.%). SU-8 photoresist (SU8-2002) is purchased from Micro Chem. Deionized water was used throughout.

A nitrate ionophore cocktail solution with a higher ionophore concentration than that of the commercial one is prepared by adding additional TDDMA to the precursor cocktail A. The concentration of the nitrate ionophore in the ISM membrane is increased from 1.5 wt.% to 6.2 wt.%.

Device Fabrication and Functionalization. The device fabrication flow is described in Figure 2a. First, a 1.5 μm thick layer of the epoxy based SU8 photoresist is spin-coated onto a silicon wafer with a 5-μm thick overgrown SiO_2 layer. Electron beam lithography (using a JEOL 8100 electron beam writer) is then used to define the geometry of the photonic structures. The photonic structures form after a precisely timed development process of the SU8 without the need for further etching. The device is then hard baked on a hotplate at 180 ˚C for 10 minutes to fully cross-link the SU8 resist to ensure that the devices have the mechanical and chemical strength to survive the functionalization process. The silicon dioxide layer optically isolates the SU8 photonic structure from the silicon substrate. The structure leverages the coupling between a race-track shaped micro-ring and a straight waveguide (see Figure 1a) that are fabricated out of cross-linked SU8 photoresist and are spaced 300-400 nm apart. The racetrack comprises of 2 semicircular sections, each with a radius of 30 μm, which are joined by two straight segments, each with a length of 200 μm. The rectangular cross-section of the waveguide and micro-ring have dimensions of 1 μm (width) x 1.1 μm (height). The waveguide extends to the edge of the chip, where it is cleaved to obtain a smooth facet for optical coupling, as shown in Figure 2c. At the edge of the chip, the waveguides are tapered to larger width (2 μm) to improve the coupling efficiency with the 4 μm core diameter single mode input fiber. A multi-mode fiber with a core diameter of 50 μm diameter is used at the output to obtain a higher collection efficiency. For practical use, the device can be packaged by carefully aligning and gluing the coupling optical fibers to the silicon chip using UV curable glue. As the final step, the device is coated with a thin layer of the nitrate ion-selective membrane. Both thin (~100 nm) and thick (~ 4 μm) coatings have been studied. For thick functionalization coatings, a droplet of precursor cocktail is placed on the device surface and a thin-film applicator is drawn across the surface to form a uniform coating. After the coating, the device is left to dry in a vented hood overnight. For thin functionalization coatings, the precursor cocktail is diluted (adding 6 ml THF to 2 ml of precursor cocktail), and then spin-coated (4000 rpm) onto the device surface, followed by drying in a vented hood overnight.

Measurements. UV-Vis measurements of optical absorption are performed using a Varian Cary 50 UV-Vis Spectrophotometer. A 100-μm-thick ion-selective membrane coated on a glass substrate was subjected to the UV-Vis measurements. Film thickness measurement is carried out by a KLA Tencor benchtop stylus profilometer. Transmission measurements are carried out by sending light from a tunable external-cavity laser (Newport TLB 6712) through the device and monitoring the output light spectrum with a 10 MHz adjustable fiber-optic receiver (New Focus

Model 2051) while the input light wavelength is scanned. Sharp resonance dips can be observed in the transmission spectrum of the straight waveguide when light evanescently couple with the racetrack resonators. For the functionalized devices, the nitrate selective exchange process alters the optical refractive index of the membrane due to the change of the local chemical environment. This, in turn, shifts the resonant peaks in the transmission spectrum of the micro-ring resonator, thereby providing an indication of the ion concentration. The nitrate concentration is changed by pipetting sodium nitrate solutions with a known concentration (0.02, 0.2, 2 ppm, etc.) in sequence to achieve desired concentrations.

2. Refractometric Measurement Results for the Photonic Sensor Functionalized by Commercial Nitrate Ionophore Cocktail

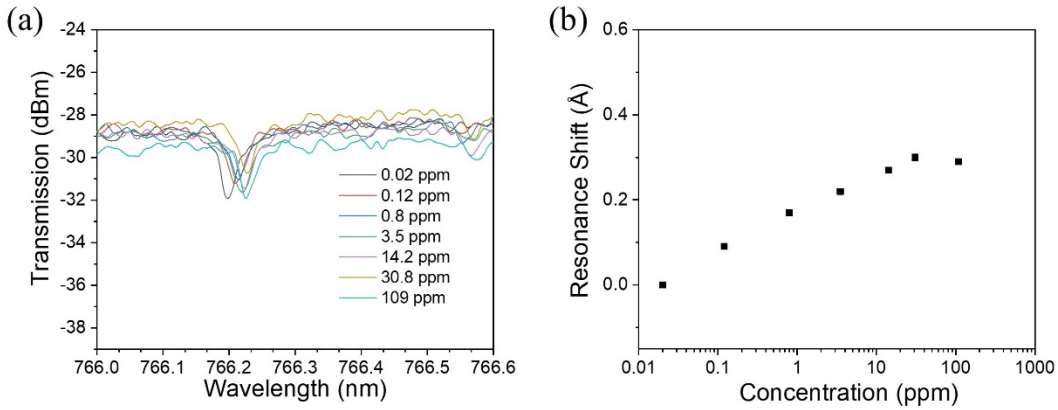

Figure S1. (a) Optical transmission spectrum of a microresonator with the functionalization coating made by the commercial nitrate ISM cocktail. (b) Measured resonance shift as a function of nitrate concentration.

A photonic sensor was functionalized by the commercial nitrate ISM and exposed to nitrate solutions with different concentrations. The resonance dip continuously shifted with increasing the nitrate concentration, while the sensitivity was limited, i.e., the total resonance shift is only around 0.3 Å when varying the nitrate concentration from 0.02 ppm to 109 ppm.

3. Study for Response Time of the Photonic Sensor

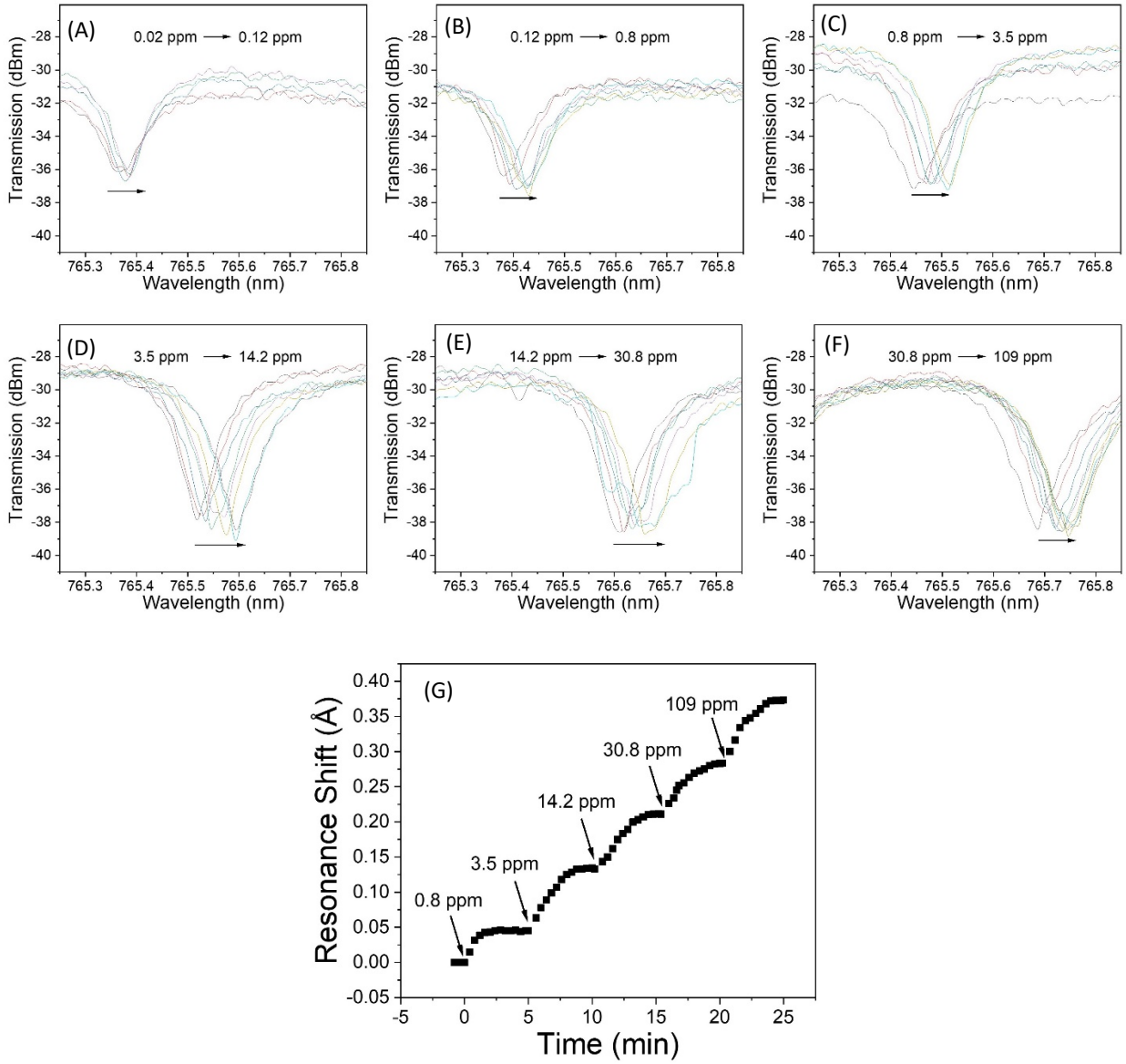

Figure S2. (A)-(F) In-situ recorded optical transmission spectrum of a nitrate-ISM-functionalized microresonator with nitrate concentration increasing. (G) Dynamic response of the sensor with the addition of NO_3^- solutions with different concentrations.

Each test was performed under the controlled experimental condition where the optical transmission spectrum was continuously recorded within a given exposure time of 5 mins after each concentration adjustment. For each test, the resonance dip gradually shifted and always stabilized within 4 minutes, indicating the relatively fast response of this ISM-functionalized photonic sensor.

4. Study for Precision of the Photonic Sensor

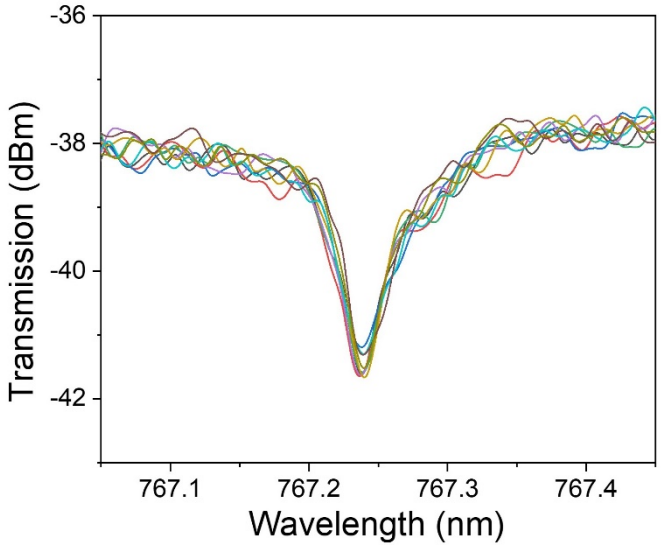

Figure S3. Spectrum of optical resonance with continuously sweeping for 10 cycles over a 4 Å range.

The nitrate-ISM-functionalized microresonator exhibits no resonance shift when the nitrate concentration is fixed (10 ppm for the measurement), reflecting the high precision of the microresonator photonic sensor.

5. Refractometric measurements of the Photonic Sensor Functionalized by Thick ISM

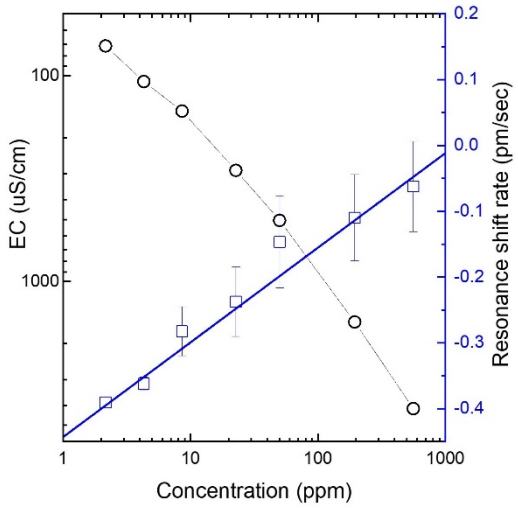

Figure S4. Measured resonance shift rate and electric conductivity as a function of nitrate concentration.